How Spherical Are Gaseous Low Charged Dendrimer Ions: A Molecular Dynamics / Ion Mobility Study?

Fabrice Saintmont[a,b], Julien De Winter[a], Fabien Chirot[c], Emilie Halin[a], Philippe Dugourd[d], Patrick Brocorens[b], Pascal Gerbaux[a*]

[a] Organic Synthesis & Mass Spectrometry Laboratory, Interdisciplinary Center for Mass Spectrometry (CISMa), Center of Innovation and Research in Materials and Polymers (CIRMAP), University of Mons - UMONS, 23 Place du Parc, 7000 Mons, Belgium

[b] Laboratory for Chemistry of Novel Materials, Center of Innovation and Research in Materials and Polymers, Research Institute for Science and Engineering of Materials, University of Mons - UMONS, 23 Place du Parc, 7000 Mons, Belgium

[c] Université Lyon, Université Claude Bernard Lyon 1, ENS de Lyon, CNRS, Institut des Sciences Analytiques, UMR 5280, 5 rue de la Doua, F-69100, Villeurbanne, France

[d] Université Lyon, Université Claude Bernard Lyon 1, CNRS, Institut Lumière Matière, F-69622, Lyon, France

[*]Corresponding Author

Supporting information

PAMAM

Table S1: Comparison between $^{TW}CCS_{N2\rightarrow He}$ and $^{DT}CCS_{He}$ for EDA and CYS PAMAM

EDA PAMAM							
G_x	charge	*m/z*	$^{TW}CCS_{N2\rightarrow He}$ (Å²)	$^{DT}CCS_{He}$ (Å²)	ΔCCS (%) [a]	$^{TW}CCS_{N2\rightarrow He}$ (Å²) single calibration	ΔCCS (%) [b]
G0	+1	517	155 ± 2	161	+3.1	166	-3.3
	+2	259	154 ± 3	159	+3.1	181	-12.1
G1	+2	715	316 ± 2	314	-1.1	309	+0.9
	+3	477	350 ± 1	335	-5.4	334	-1.0
G2	+3	1086	539 ± 2	542	+0.6	531	+2.1
	+4	818	586 ± 2	598	+2.0	571	+4.7
	+5	652	662 ± 3	657	-0.7	636	+3.2
CYS PAMAM							
G_x	charge	*m/z*	$^{TW}CCS_{N2\rightarrow He}$ (Å²)	$^{DT}CCS_{He}$ (Å²)	ΔCCS (%) [a]	$^{TW}CCS_{N2\rightarrow He}$ (Å²) single calibration	ΔCCS (%) [b]
G0	+1	609	169 ± 2	169	-0.6	179	-5.6
	+2	305	177 ± 3	170	-5.5	196	-13.1
G1	+2	762	327 ± 2	320	-2.0	320	-0.2
	+3	508	368 ± 1	343	-6.7	353	-2.7
G2	+3	1116	546 ± 2	550	+0.7	538	+2.2
	+4	838	605 ± 1	612	+1.1	591	+3.6
	+5	671	680 ± 3	679	-0.2	661	+2.7
	+6	559	759 ± 3	773	+1.8	726	+6.5
G3	+4	1751	864 ± 12	864	-0.1	849	+1.8
	+5	1401	901 ± 14	925	+2.7	880	+5.1
	+6	1168	1013 ± 14	1046	+3.3	982	+6.5
	+7	1001	1101 ± 9	1144	+3.9	1076	+6.3

[a] $\Delta CCS = {}^{DT}CCS_{He} - {}^{TW}CCS_{N2\rightarrow He}$ | [b] $\Delta CCS = {}^{DT}CCS_{He} - {}^{TW}CCS_{N2\rightarrow He}$ (single calibration)

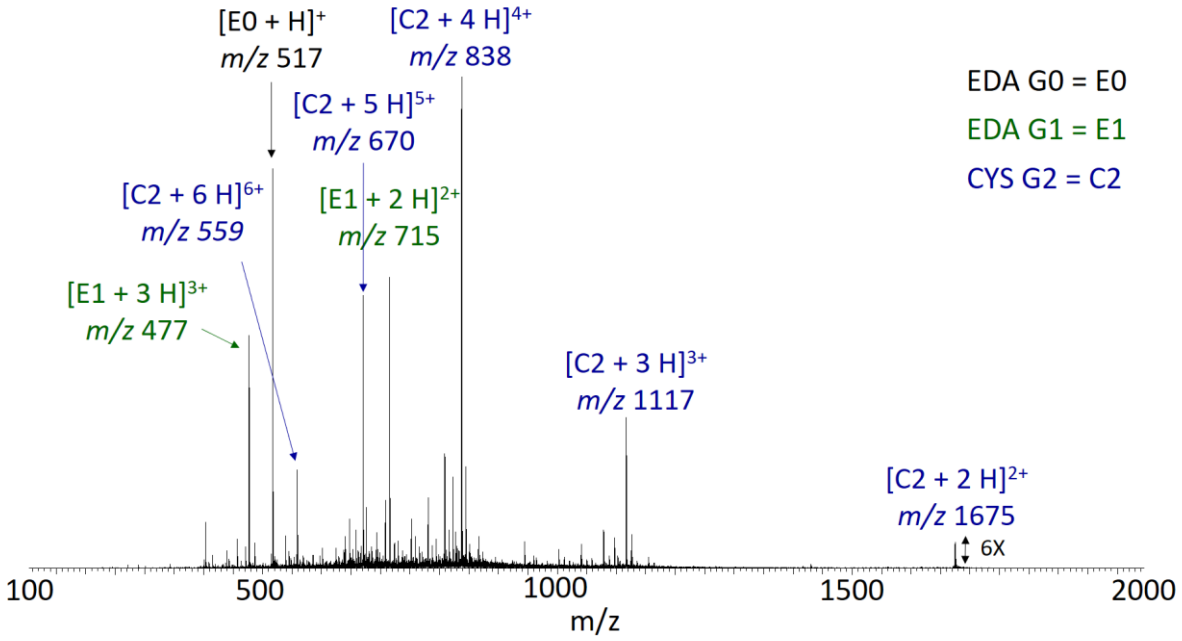

Figure S1: ESI(+)-MS spectrum of CYS PAMAM G2 dendrimer (C2). EDA PAMAM G1 (E1) and G0 (E0) are also present as a synthesis impurity.

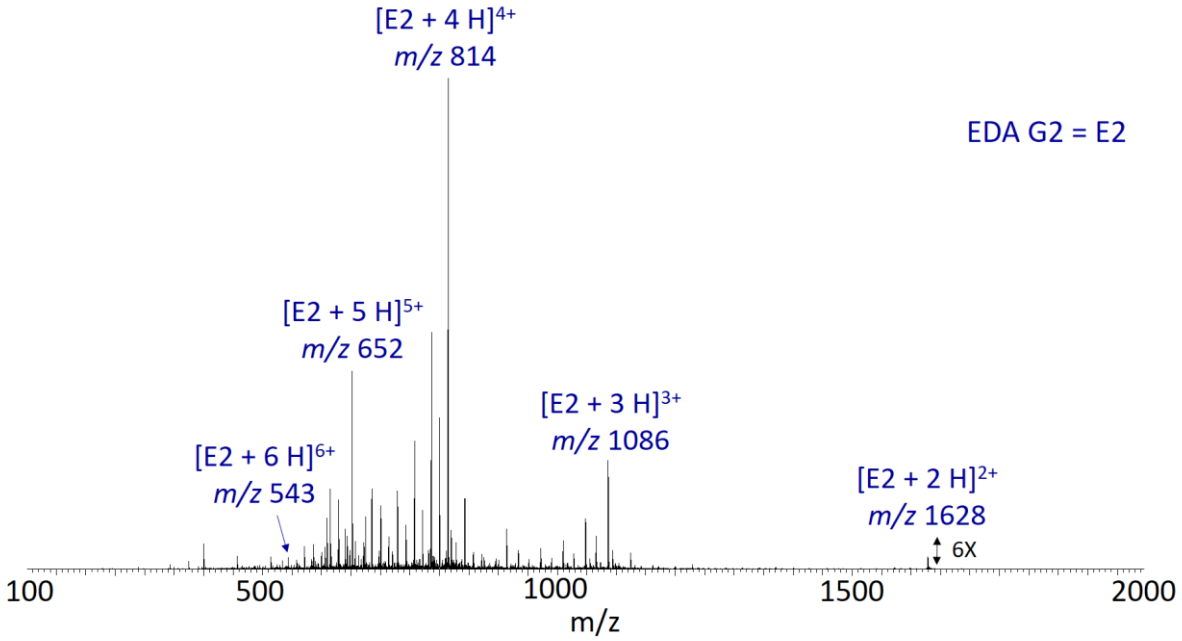

Figure S2: ESI(+)-MS spectrum of EDA PAMAM G2 dendrimer (E2). Peaks at lower m/z are typical from molecular loop (-60 u) and missing arm (-114 u) [1].

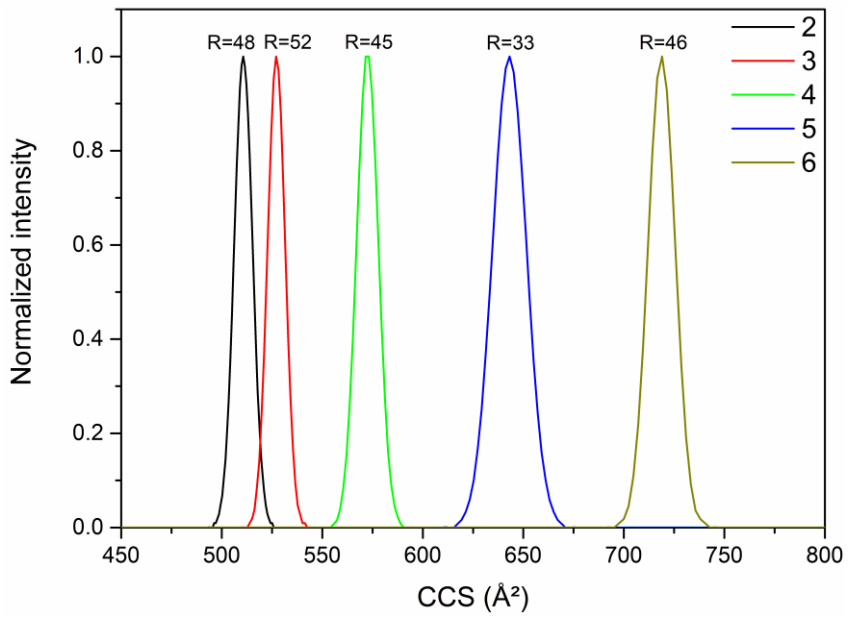

Figure S3: Evolution of CCS distribution with the number of charges (2+ to 6+) for EDA G2. The CCS resolution of each peak is indicated.

Table S2: Experimental and theoretical CCS of PAMAM ions.

EDA PAMAM					
G_x	charge	m/z	$^{TW}CCS_{N2\rightarrow He}$ (Å^2)	$^{TM}CCS_{He}$ (Å^2)	ΔCCS (%) [a]
G0	+1	517	155 ± 2	145 ± 2	-6.5
	+2	259	154 ± 3	155 ± 1	+0.4
G1	+1	1430	308 ± 2	279 ± 3	-9.5
	+2	715	316 ± 2	292 ± 3	-7.6
	+3	477	350 ± 1	341 ± 5	-2.7
	+4	358	417 ± 1	366 ± 4	-12.2
G2	+2	1629	521 ± 2	505 ± 6	-3.1
	+3	1086	539 ± 2	519 ± 6	-3.6
	+4	818	586 ± 3	557 ± 6	-4.9
	+5	652	662 ± 1	625 ± 8	-5.5
	+6	544	738 ± 1	722 ± 7	-2.3
G3	+4	1728	847 ± 7	843 ± 7	-0.4
	+5	1383	883 ± 8	908 ± 9	+2.8
	+6	1152	967 ± 6	976 ± 9	+1.0
	+7	988	1054 ± 8	1052 ± 8	-0.2
CYS PAMAM					
G_x	charge	m/z	$^{TW}CCS_{N2\rightarrow He}$ (Å^2)	$^{TM}CCS_{He}$ (Å^2)	ΔCCS (%)
G0	+1	609	169 ± 2	162 ± 2	-4.2

	+2	305	177 ± 3	168 ± 2	-4.9
G1	+1	1522	324 ± 2	289 ± 3	-10.7
	+2	762	327 ± 2	305 ± 3	-6.7
	+3	508	368 ± 1	357 ± 5	-3.0
	+4	381	432 ± 2	417 ± 5	-3.4
G2	+2	1675	529 ± 2	521 ± 5	-1.5
	+3	1116	546 ± 2	568 ± 5	+4.0
	+4	838	605 ± 1	610 ± 8	+0.8
	+5	671	680 ± 3	659 ± 6	-3.2
	+6	559	759 ± 3	698 ± 8	-8.0
G3	+4	1751	864 ± 12	841 ± 8	-2.8
	+5	1401	901 ± 14	895 ± 9	-0.7
	+6	1168	1013 ± 14	1046 ± 12	+3.3
	+7	1001	1101 ± 19	1103 ± 8	+0.2
[a] $\Delta CCS = {}^{TM}CCS_{He} - {}^{TW}CCS_{N2\rightarrow He}$					

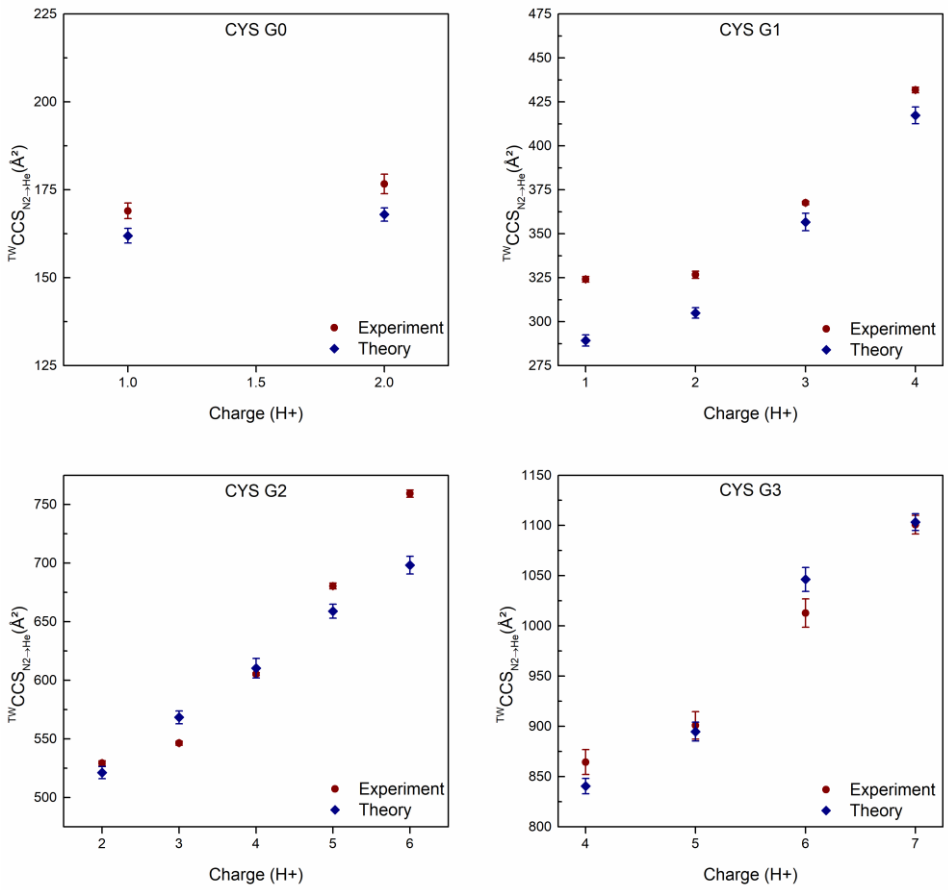

Figure S4: Comparison between experimental (red circle) and theoretical (blue diamond) CCS for CYS PAMAM G0 to G3. Error bars represent the standard deviation on 5 (G0) or 3 (G1 to G3) experimental measurements, and on 200 theoretical structures, respectively.

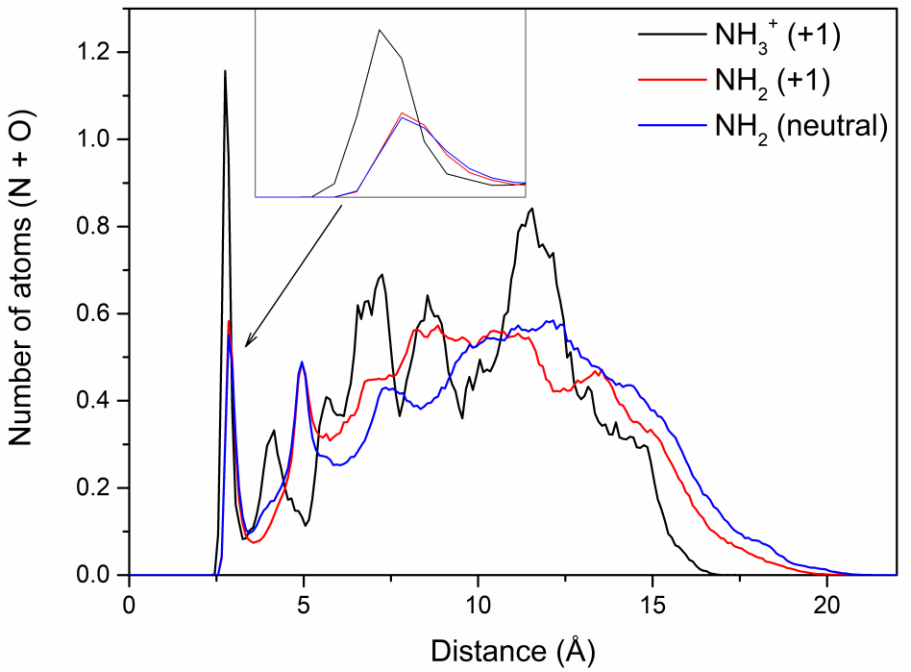

Figure S5: Number of oxygen atoms and amine nitrogen atoms found in concentric shells 0.1 Å thick, as a function of the distance from terminal amine nitrogens in EDA G2 neutral and +1. For the neutral, the curve is the average over all the terminal amines (blue). For the +1, the averages over all the neutral amines (red) and the protonated amine (black) are separated. A zoom between 2.2 and 3.4 Å is in insert.

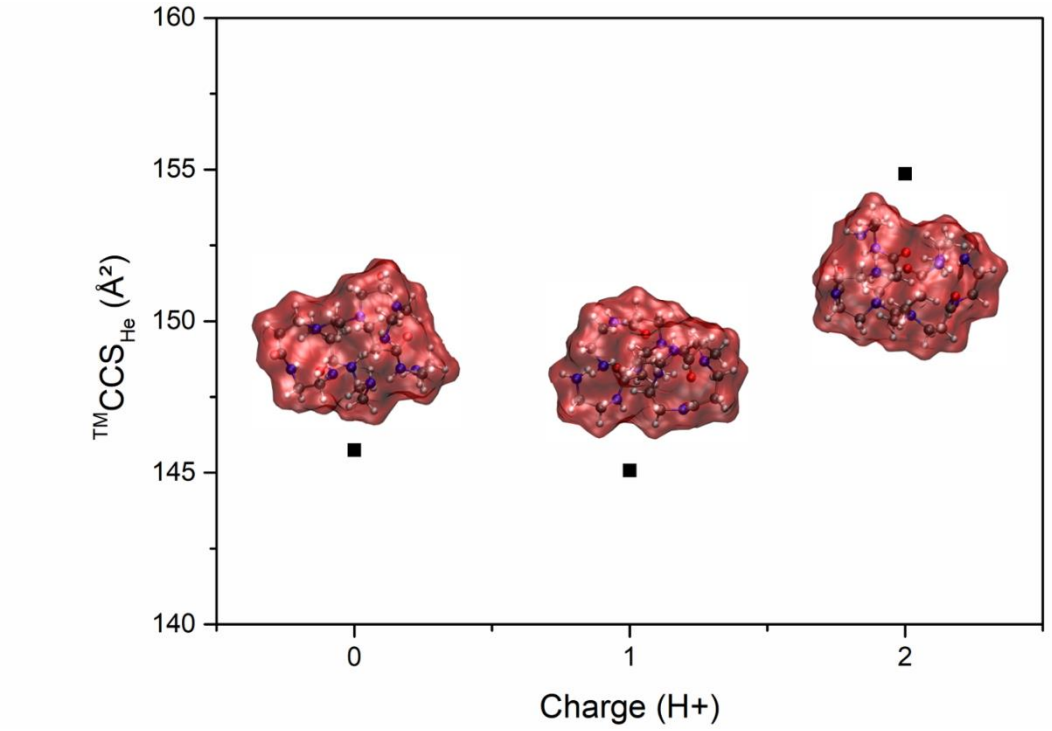

Figure S6: Evolution of the $^{TM}CCS_{He}$ for EDA PAMAM G0 from 0 to 2 charges. For each charge state, the structure is represented with the vdW surface in red.

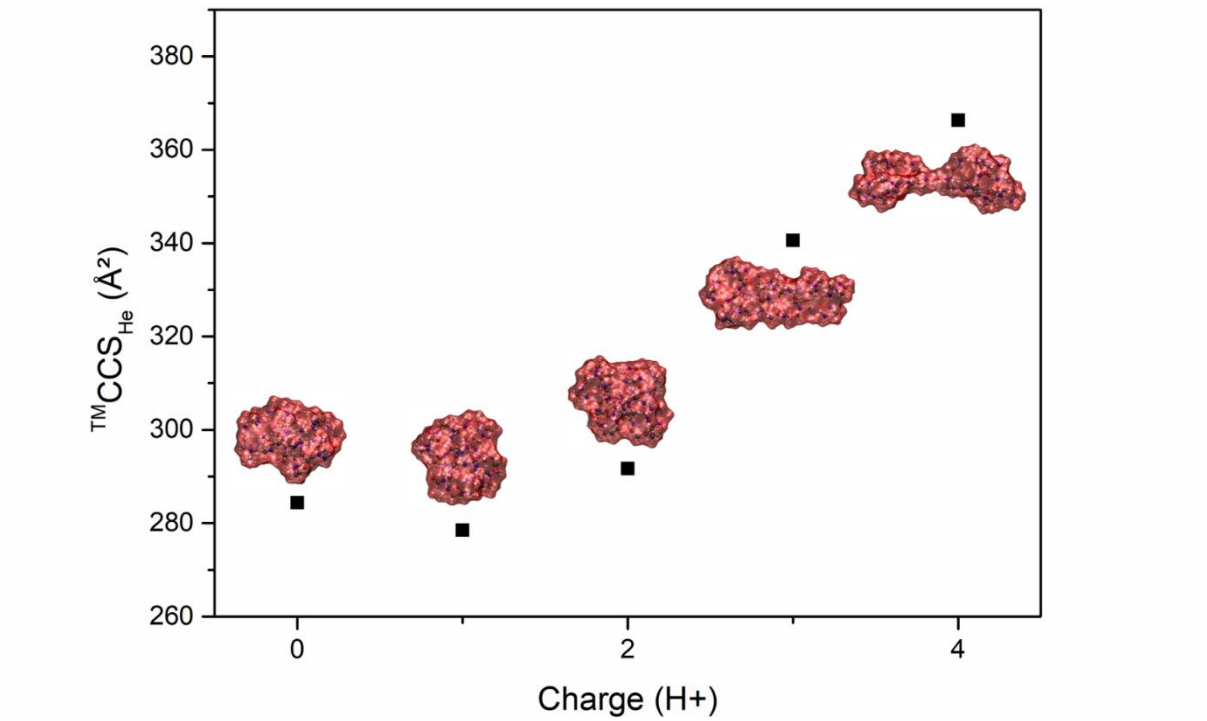

Figure S7: Evolution of the $^{TM}CCS_{He}$ for EDA PAMAM G1 from 0 to 4 charges. For each charge state, the structure is represented with the vdW surface in red.

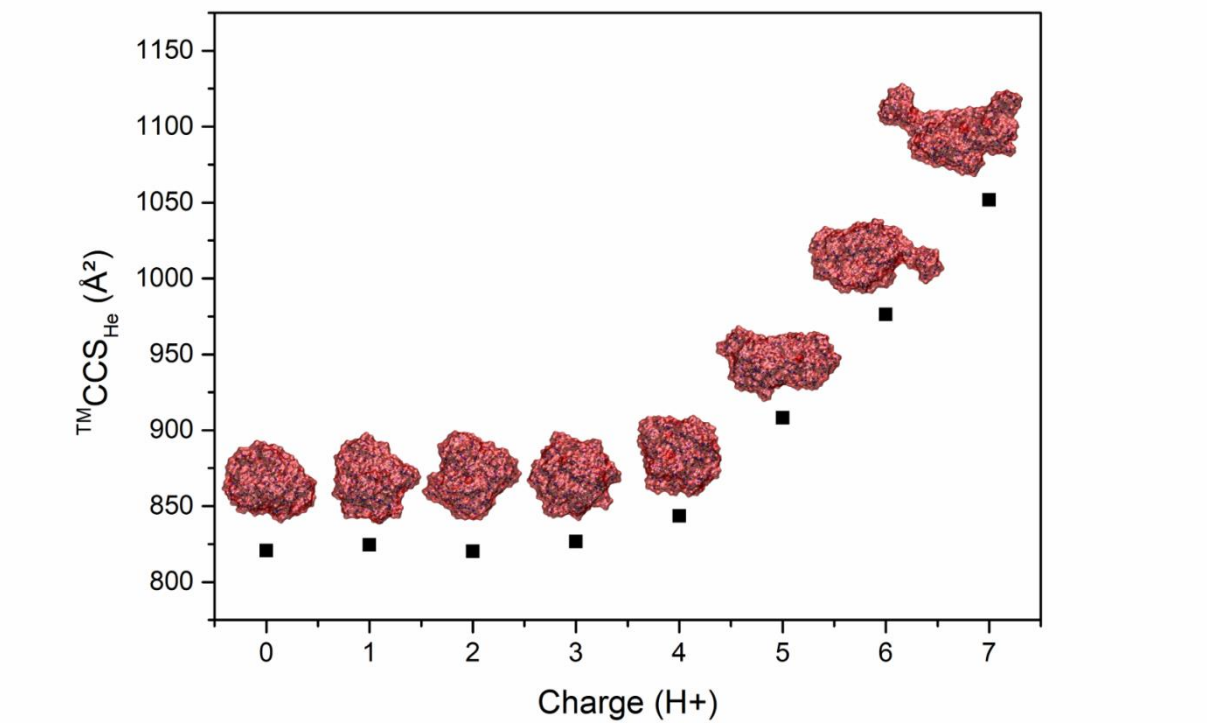

Figure S8: Evolution of the $^{TM}CCS_{He}$ for EDA PAMAM G3 from 0 to 7 charges. For each charge state, the structure is represented with the vdW surface in red.

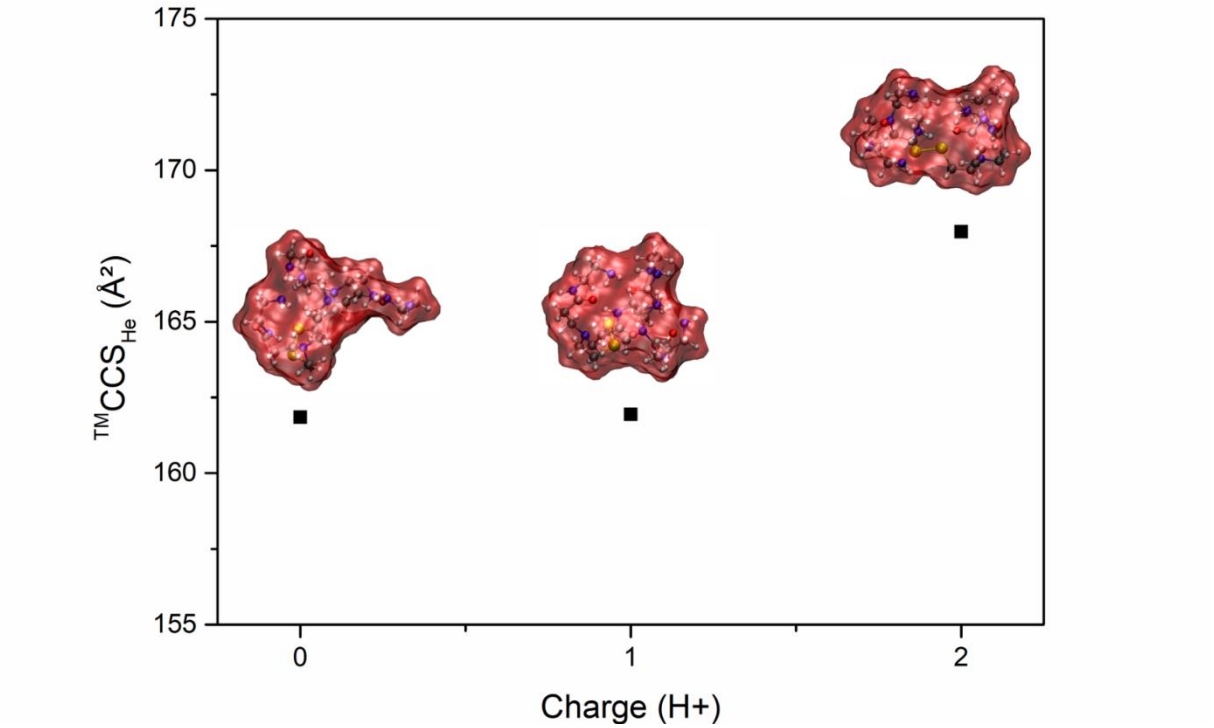

Figure S9: Evolution of the $^{TM}CCS_{He}$ for CYS PAMAM G0 from 0 to 2 charges. For each charge state, the structure is represented with the vdW surface in red.

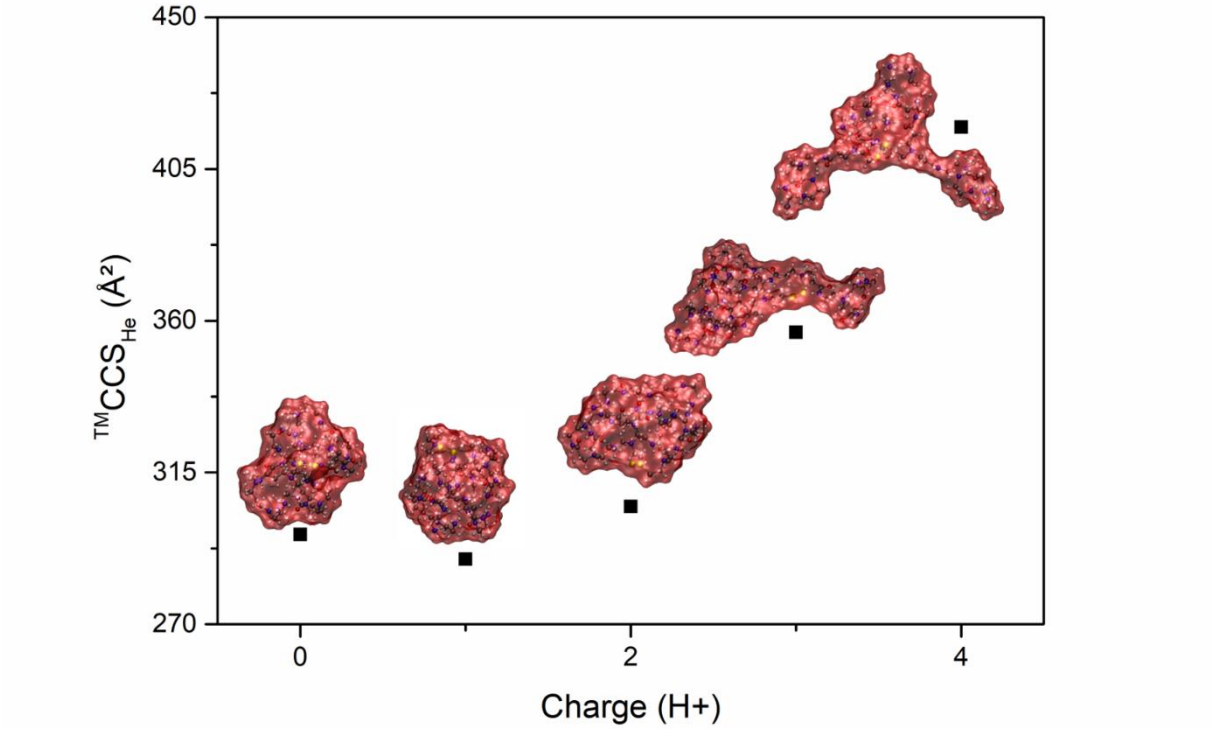

Figure S10: Evolution of the $^{TM}CCS_{He}$ for CYS PAMAM G1 from 0 to 4 charges. For each charge state, the structure is represented with the vdW surface in red.

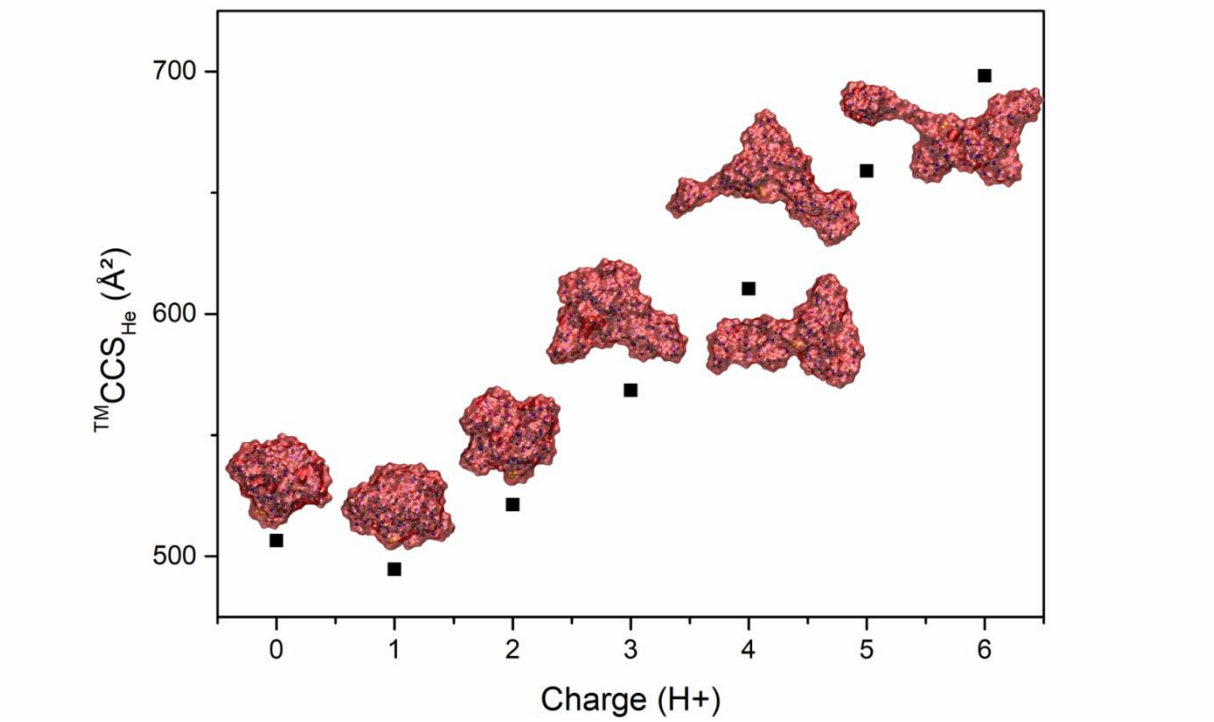

Figure S11: Evolution of the $^{TM}CCS_{He}$ for CYS PAMAM G2 from 0 to 6 charges. For each charge state, the structure is represented with the vdW surface in red.

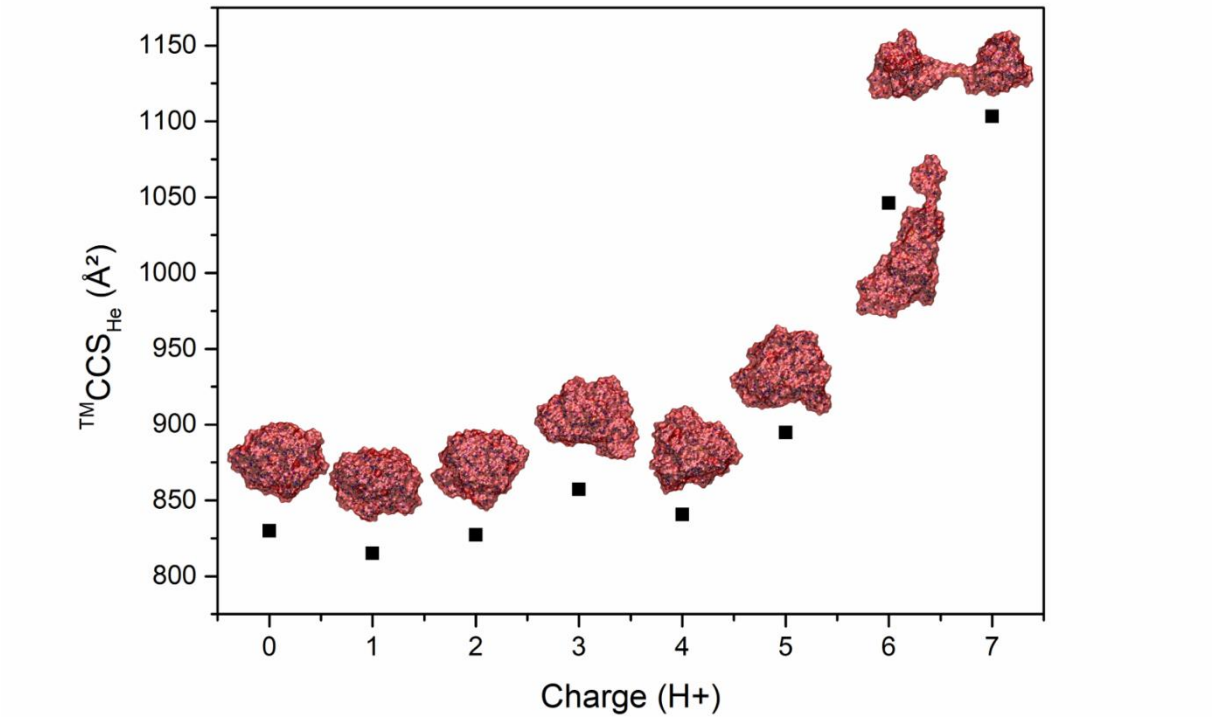

Figure S12: Evolution of the $^{TM}CCS_{He}$ for CYS PAMAM G3 from 0 to 7 charges. For each charge state, the structure is represented with the vdW surface in red.

Table S3: Molecular dynamics simulation of the globular PAMAM ions and neutrals: theoretical CCS, SASA, V_{SASA} and corresponding densities.

EDA PAMAM							
G_x	Charge	MW (Da)	$^{TM}CCS_{He}$ (Å^2)	SASA (Å^2)	V_{SASA} (Å^3)	ρ_{SASA} (Da/Å^3) [a]	ρ_{CCS} (Da/Å^3) [a,b]
G0	0	516	146	673	1329	0.39 (0.65)	0.39 (0.65)
	+1	517	145	663	1315	0.39 (0.65)	0.39 (0.65)
	+2	518	155	676	1339	0.39 (0.65)	0.36 (0.60)
G1	0	1429	284	1219	3080	0.46 (0.76)	0.40 (0.66)
	+1	1430	279	1217	3080	0.46 (0.76)	0.41 (0.68)
	+2	1431	292	1257	3119	0.46 (0.76)	0.38 (0.63)
G2	0	3255	505	2153	6524	0.50 (0.83)	0.38 (0.63)
	+1	3256	489	2050	6366	0.51 (0.85)	0.40 (0.66)
	+2	3257	505	2122	6422	0.51 (0.85)	0.38 (0.63)
	+3	3258	519	2209	6607	0.49 (0.81)	0.37 (0.61)
G3	0	6908	821	3354	12678	0.54 (0.91)	0.39 (0.65)
	+1	6909	824	3406	12656	0.55 (0.90)	0.39 (0.65)
	+2	6910	820	3322	12499	0.55 (0.90)	0.39 (0.65)
	+3	6911	827	3427	12876	0.54 (0.91)	0.39 (0.65)
	+4	6912	843	3427	12796	0.54 (0.91)	0.38 (0.63)
CYS PAMAM							
G_x	Charge	MW (Da)	$^{TM}CCS_{He}$ (Å^2)	SASA (Å^2)	V_{SASA} (Å^3)	ρ_{SASA} (Da/Å^3) [a]	ρ_{CCS} (Da/Å^3) [a,b]
G0	0	608	162	770	1539	0.40 (0.66)	0.39 (0.65)
	+1	609	162	738	1496	0.41 (0.68)	0.39 (0.65)
	+2	610	168	758	1519	0.40 (0.66)	0.37 (0.61)
G1	0	1521	297	1295	3299	0.46 (0.76)	0.40 (0.66)
	+1	1522	289	1251	3267	0.47 (0.78)	0.41 (0.68)
	+2	1523	305	1326	3314	0.46 (0.76)	0.38 (0.63)
G2	0	3348	507	2107	6601	0.51 (0.85)	0.39 (0.65)
	+1	3349	495	2059	6498	0.52 (0.86)	0.40 (0.66)
	+2	3350	521	2191	6723	0.50 (0.83)	0.37 (0.61)
G3	0	7001	830	3404	12847	0.54 (0.91)	0.39 (0.65)
	+1	7002	815	3319	12719	0.55 (0.90)	0.40 (0.66)
	+2	7003	827	3377	12819	0.55 (0.90)	0.39 (0.65)
	+3	7004	857	3579	13026	0.54 (0.91)	0.37 (0.61)
	+4	7005	841	3508	13053	0.54 (0.91)	0.38 (0.63)

[a] the values in parenthesis are in g/cm³ | [b] the CCS-based densities are calculated based on the $^{TM}CCS_{He}$

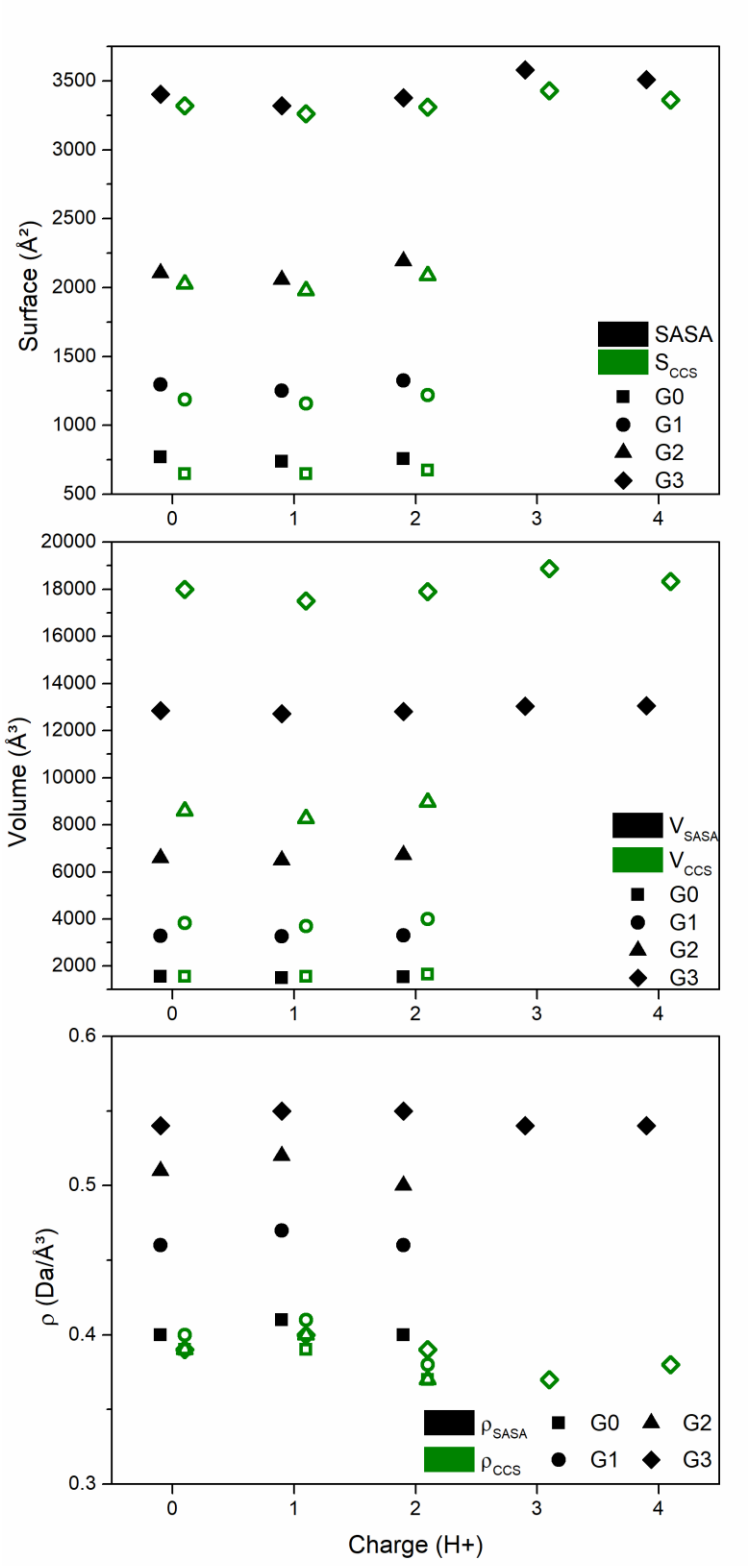

Figure S13: Comparison between surfaces (top), volumes (middle) and densities (bottom) from the last frame of the MD (black, solid) and calculated based on the average $^{TM}CCS_{He}$ on 200 frames (green, hollow) of CYS PAMAM ions and neutrals for G0 to G3.

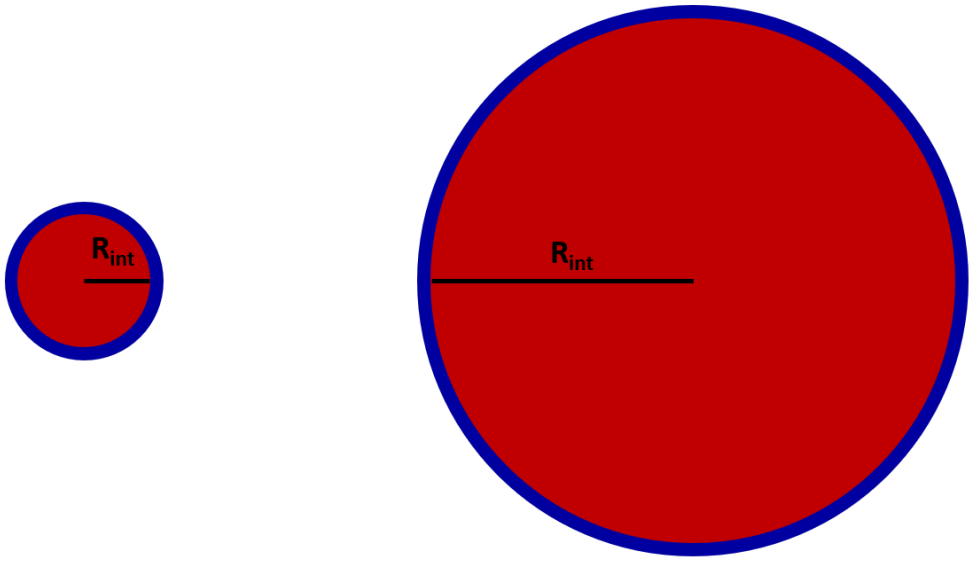

$R_{int} = 5$
$V_{tot} = 905$
$V_{shell} = 381$
42%

$R_{probe} = 1$

$R_{int} = 20$
$V_{tot} = 38792$
$V_{shell} = 5282$
14%

$$V_{tot} = \frac{4\pi}{3}(R_{int} + R_{probe})^3 \qquad V_{shell} = \frac{4\pi}{3}\left(3R_{int}{}^2 R_{probe} + 3R_{int}(R_{probe})^2 + (R_{probe})^3\right)$$

Figure S14: Representation of the extra volume due to the probe decreasing with the radius of the molecule. For a probe radius of 1 in arbitrary units, the shell represents 42% of the total volume for an internal radius of 5 while it represents only 14% for an internal radius of 20. For the development of the equation for the V_{shell} calculation, see the end of the SI.

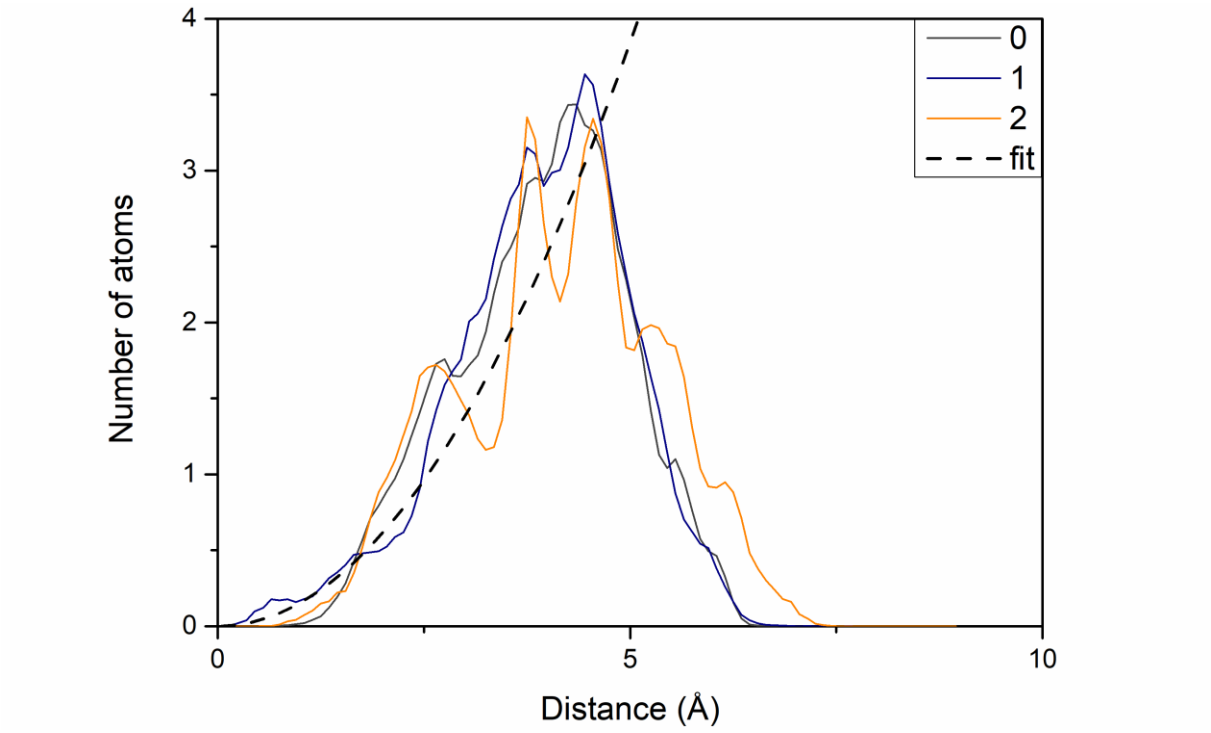

Figure S15: Number of atoms found in concentric shells 0.1 Å thick, as a function of the distance from the geometrical center. Results of EDA G0, for charge states 0 to +2. The average parabolic fit corresponding to a dense core model is displayed in dashed lines. The fit for all the generations differs from the curves for G0.

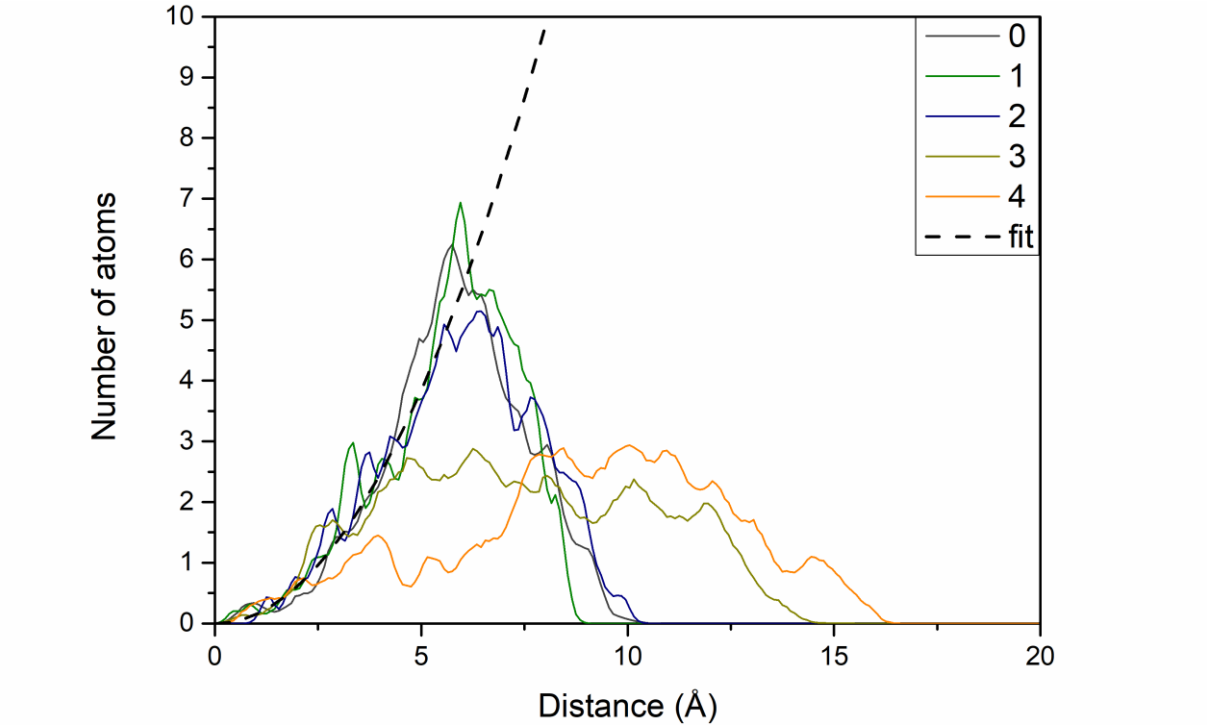

Figure S16: Number of atoms found in concentric shells 0.1 Å thick, as a function of the distance from the geometrical center. Results of EDA G1, for charge states 0 to +4. A parabolic fit corresponding to a dense core model is displayed in dashed lines.

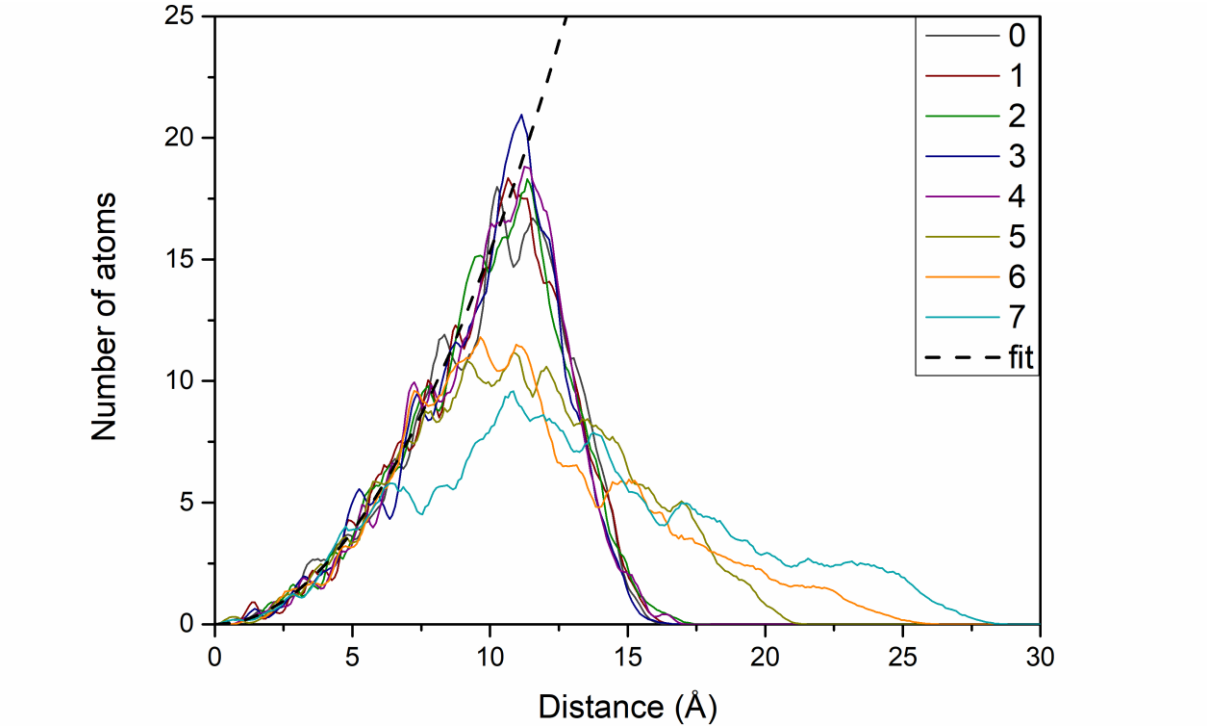

Figure S17: Number of atoms found in concentric shells 0.1 Å thick, as a function of the distance from the geometrical center. Results of EDA G3, for charge states 0 to +7. A parabolic fit corresponding to a dense core model is displayed in dashed lines.

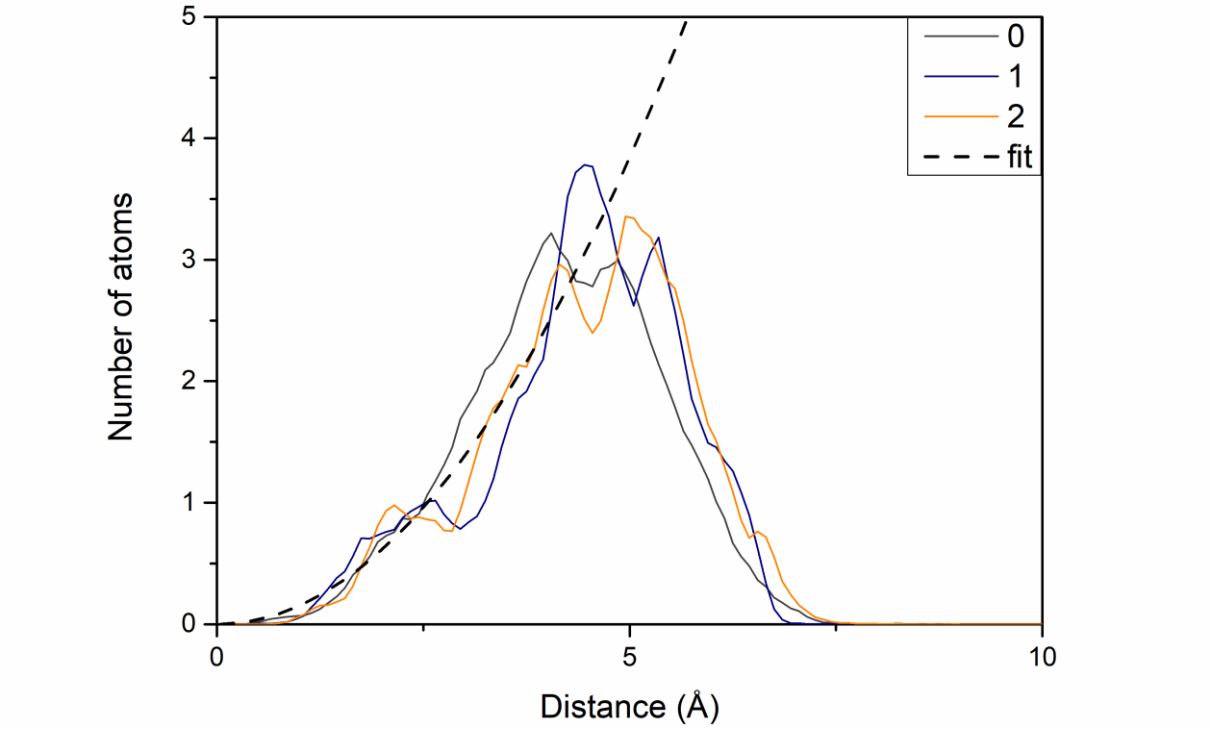

Figure S18: Number of atoms found in concentric shells 0.1 Å thick, as a function of the distance from the geometrical center. Results of CYS G0, for charge states 0 to +2. The average parabolic fit corresponding to a dense core model is displayed in dashed lines. The fit for all the generations differs from the curves for G0.

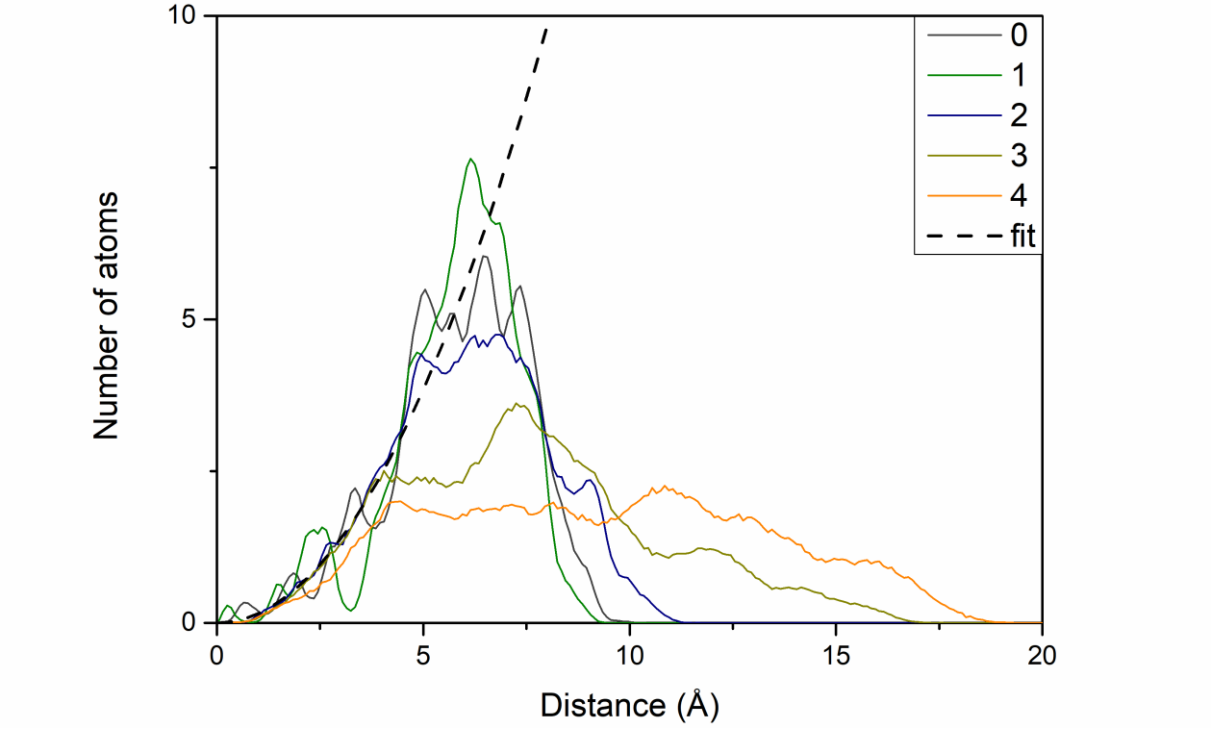

Figure S19: Number of atoms found in concentric shells 0.1 Å thick, as a function of the distance from the geometrical center. Results of CYS G1, for charge states 0 to +4. A parabolic fit corresponding to a dense core model is displayed in dashed lines.

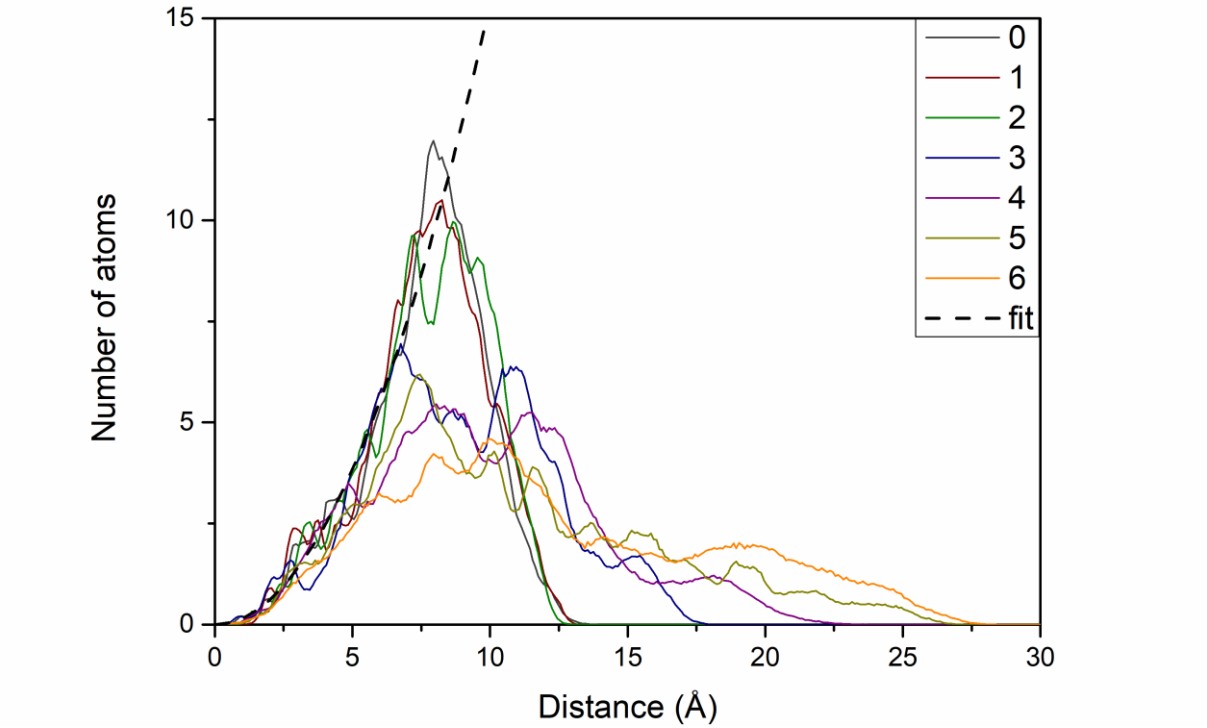

Figure S20: Number of atoms found in concentric shells 0.1 Å thick, as a function of the distance from the geometrical center. Results of CYS G2, for charge states 0 to +6. A parabolic fit corresponding to a dense core model is displayed in dashed lines.

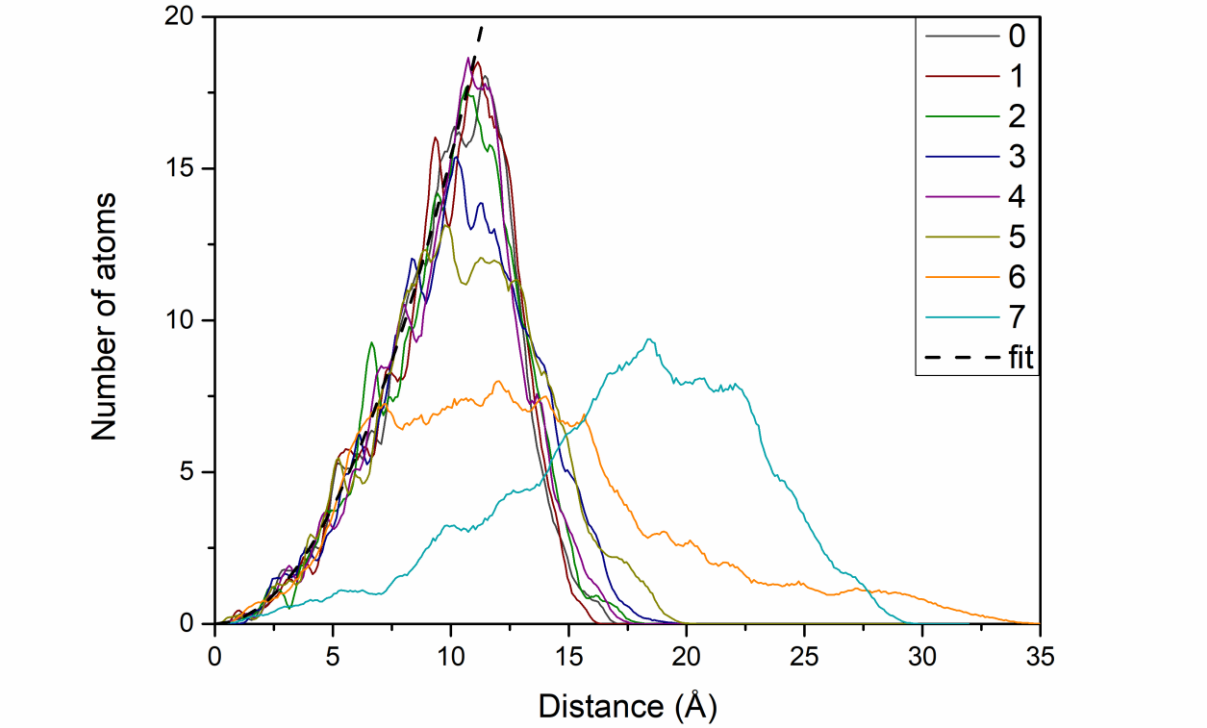

Figure S21: Number of atoms found in concentric shells 0.1 Å thick, as a function of the distance from the geometrical center. Results of CYS G3, for charge states 0 to +7. A parabolic fit corresponding to a dense core model is displayed in dashed lines.

PPI

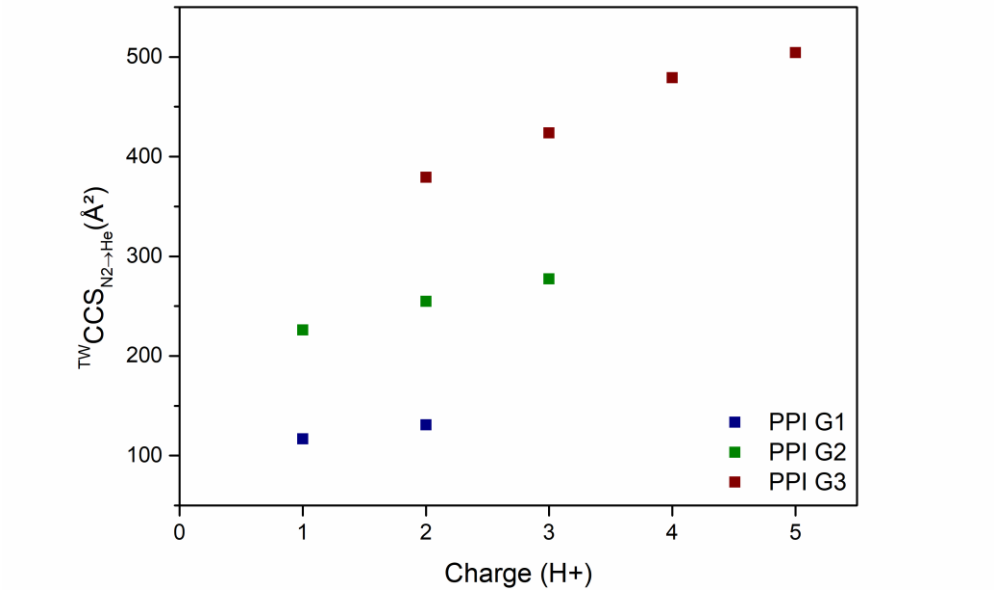

Figure S22: Evolution of the experimental $^{TW}CCS_{N2\rightarrow He}$ as a function of the charge state for PPI from G1 to G3.

Table S4: $^{TW}CCS_{N2\rightarrow He}$ and $^{DT}CCS_{He}$ of PPI ions

PPI							
G_x	charge	*m/z*	$^{TW}CCS_{N2\rightarrow He}$ (Å²)	$^{DT}CCS_{He}$ (Å²)	ΔCCS (%) [a]	$^{TW}CCS_{N2\rightarrow He}$ (Å²) single calibration	ΔCCS (%) [b]
G1	+1	317	117 ± 2	123	+4.8	129	+10.3
	+2	159	131 ± 4	139	+6.1	150	+14.5
G2	+2	387	255 ± 2	256	+0.6	247	-3.0
	+3	259	277 ± 4	272	-2.0	266	-4.2
G3	+3	563	424 ± 3	444	+4.7	412	-2.7
	+4	423	479 ± 4	504	+5.2	458	-4.4
[a] ΔCCS = $^{DT}CCS_{He}$ - $^{TW}CCS_{N2\rightarrow He}$ | [b] ΔCCS = $^{DT}CCS_{He}$ - $^{TW}CCS_{N2\rightarrow He}$ (single calibration)							

Table S5: Experimental and theoretical CCS of PPI ions.

PPI					
G_x	charge	*m/z*	$^{TW}CCS_{N2\rightarrow He}$ (Å²)	$^{TM}CCS_{He}$ (Å²)	ΔCCS (%)
G1	+1	317	117 ± 2	115 ± 2	1.8
	+2	159	131 ± 4	138 ± 1	5.7
G2	+1	774	226 ± 1	216 ± 6	4.4
	+2	387	255 ± 2	249 ± 4	2.4
	+3	259	277 ± 4	268 ± 5	3.4
G3	+2	844	379 ± 1	378 ± 8	0.4
	+3	563	424 ± 3	424 ± 7	0.0
	+4	423	479 ± 4	499 ± 8	4.1
	+5	338	504 ± 4	519 ± 7	2.9

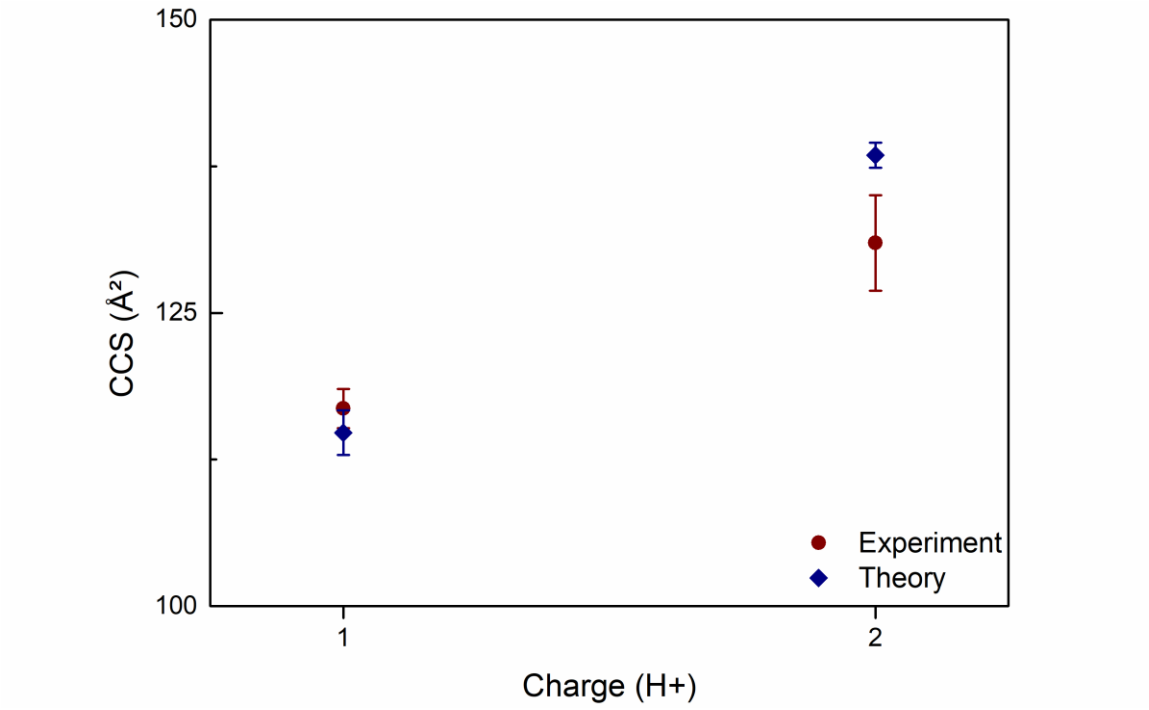

Figure S23: Comparison between experimental (red circle) and theoretical (blue diamond) CCS for PPI G1. Error bars represent the standard deviation on 5 experimental measurements, and on 200 theoretical structures, respectively.

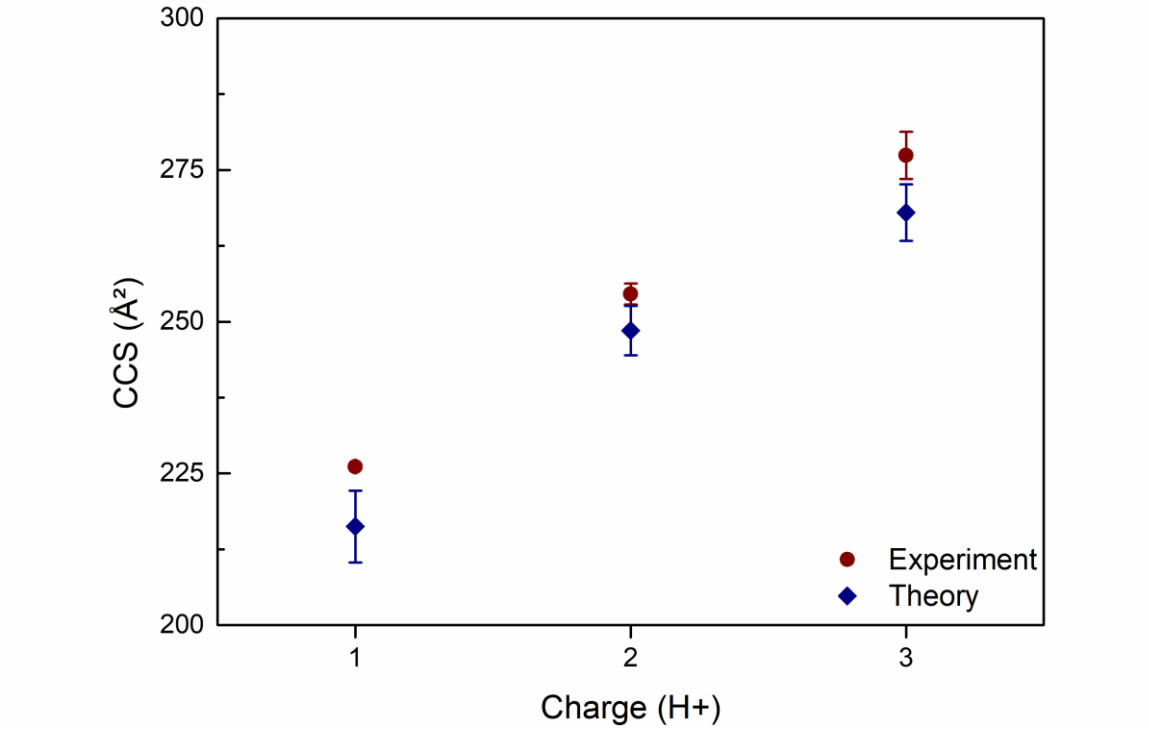

Figure S24: Comparison between experimental (red circle) and theoretical (blue diamond) CCS for PPI G2. Error bars represent the standard deviation on 3 experimental measurements, and on 200 theoretical structures, respectively.

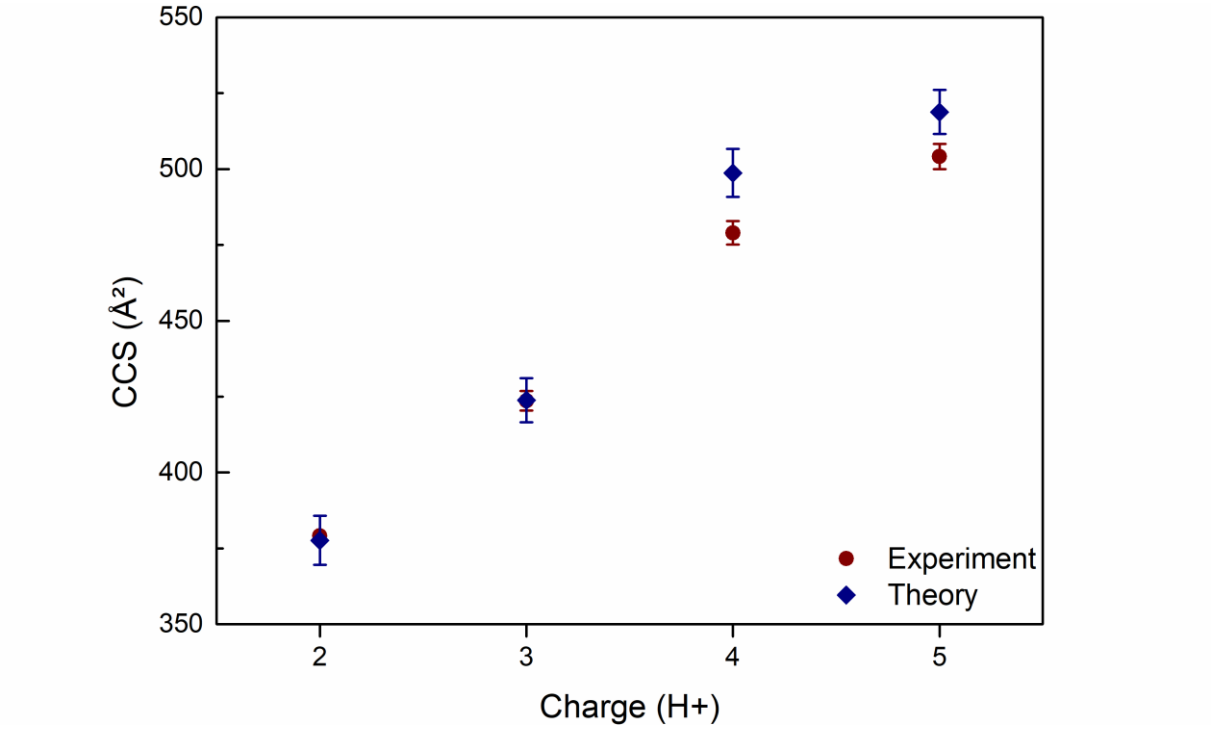

Figure S25: Comparison between experimental (red circle) and theoretical (blue diamond) CCS for PPI G3. Error bars represent the standard deviation on 3 experimental measurements, and on 200 theoretical structures, respectively.

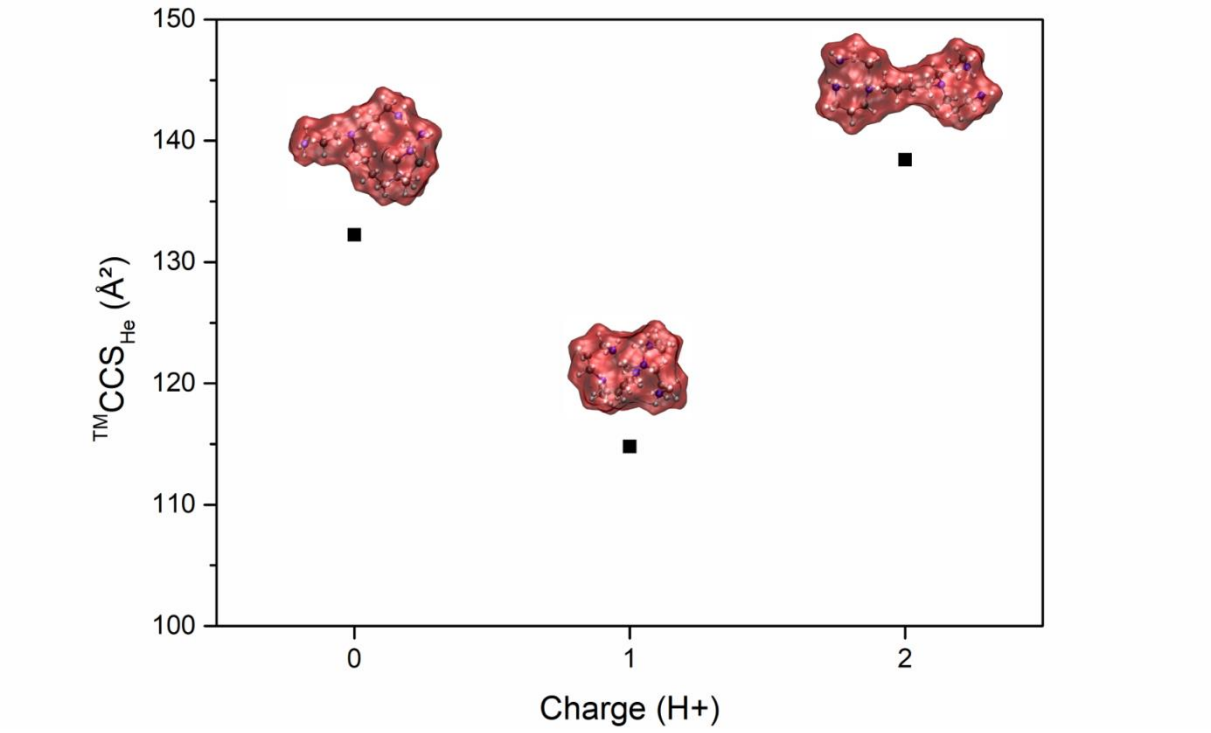

Figure S26: Evolution of the theoretical $^{TM}CCS_{He}$ for PPI G1 from 0 to 2 charges. For each charge state, the structure is represented with the Connolly surface in red.

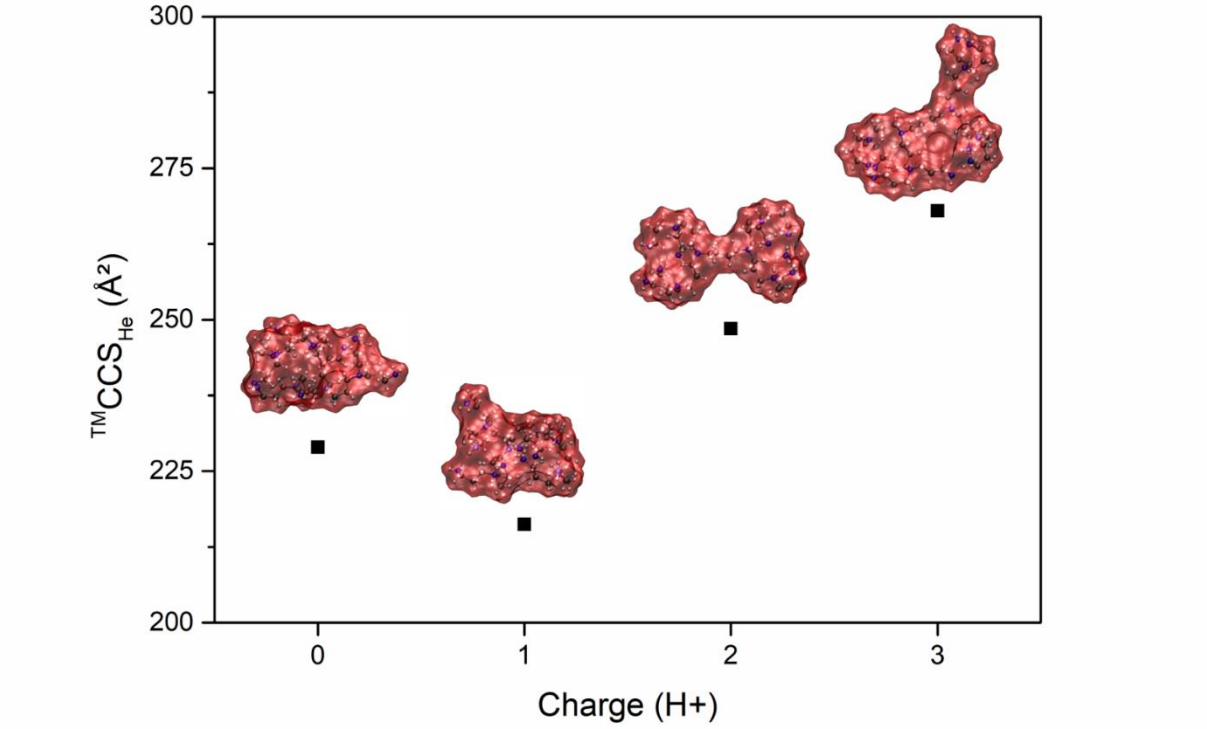

Figure S27: Evolution of the theoretical $^{TM}CCS_{He}$ for PPI G2 from 0 to 3 charges. For each charge state, the structure is represented with the Connolly surface in red.

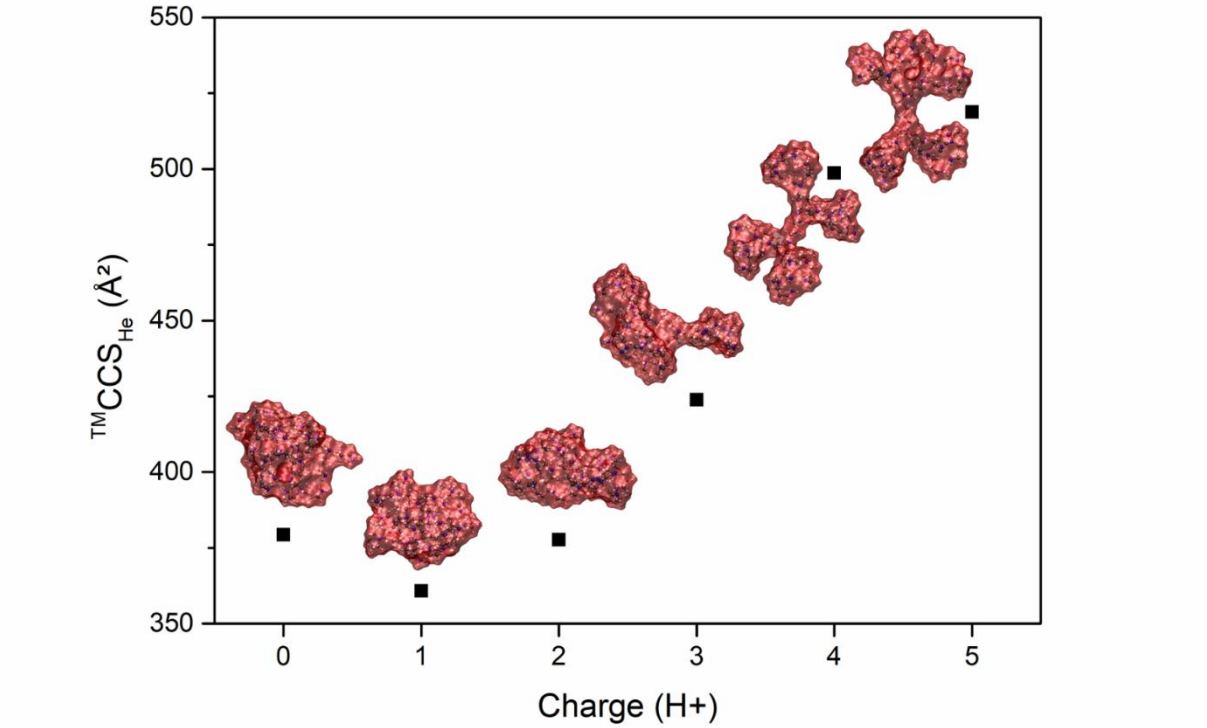

Figure S28: Evolution of the theoretical $^{TM}CCS_{He}$ for PPI G3 from 0 to 5 charges. For each charge state, the structure is represented with the Connolly surface in red.

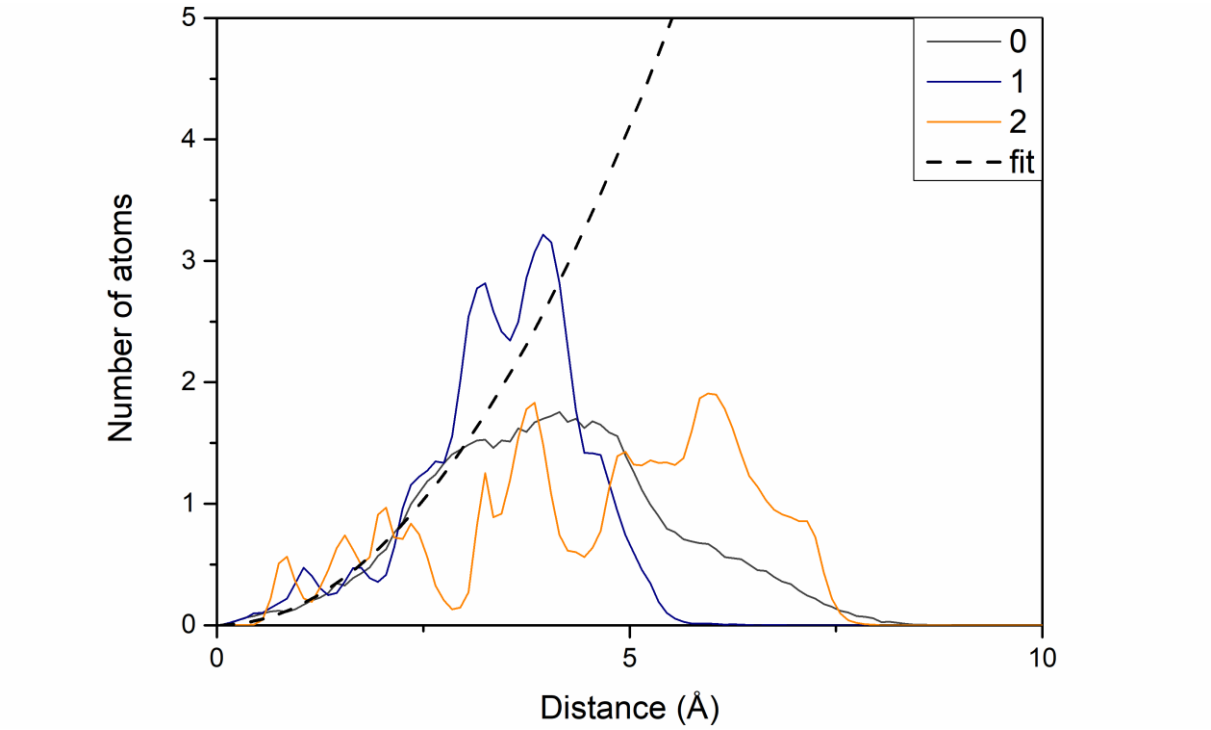

Figure S29: Number of atoms found in concentric shells 0.1 Å thick, as a function of the distance from the geometrical center. Results of PPI G1, for charge states 0 to +2. The average parabolic fit corresponding to a dense core model is displayed in dashed lines. The fit for all the generations differs from the curves for G1.

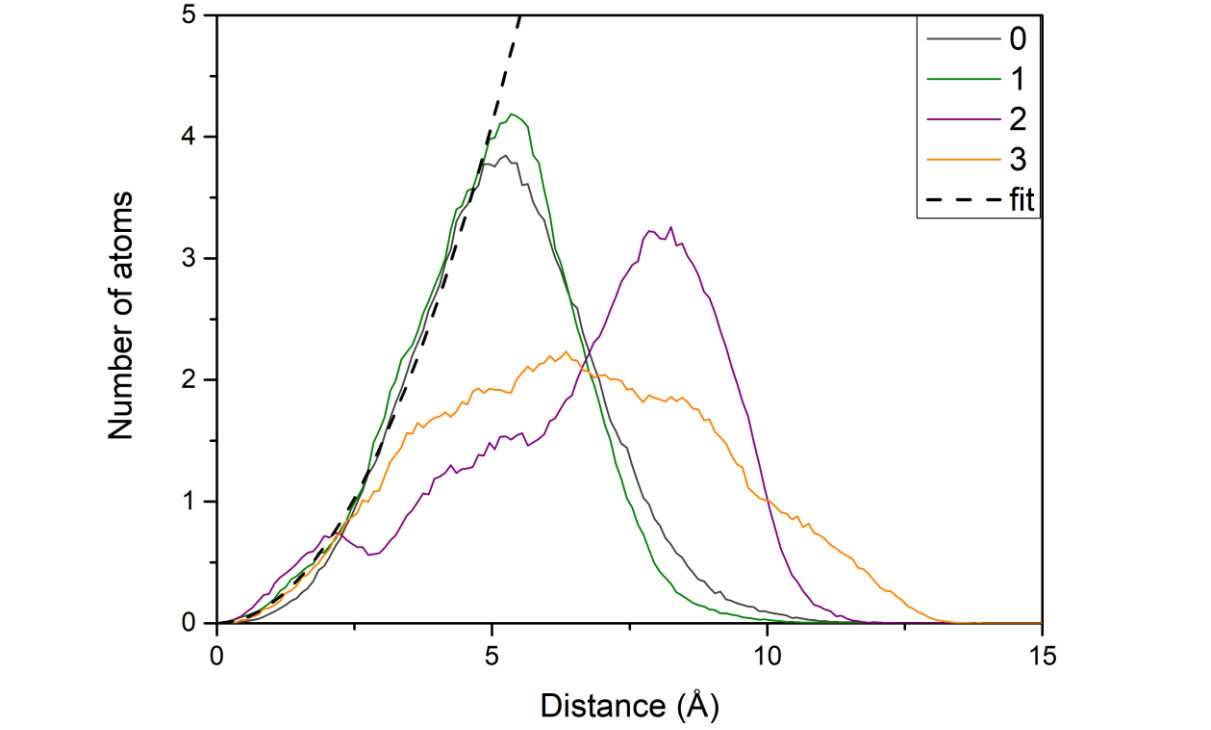

Figure S30: Number of atoms found in concentric shells 0.1 Å thick, as a function of the distance from the geometrical center. Results of PPI G2, for charge states 0 to +3. A parabolic fit corresponding to a dense core model is displayed in dashed lines.

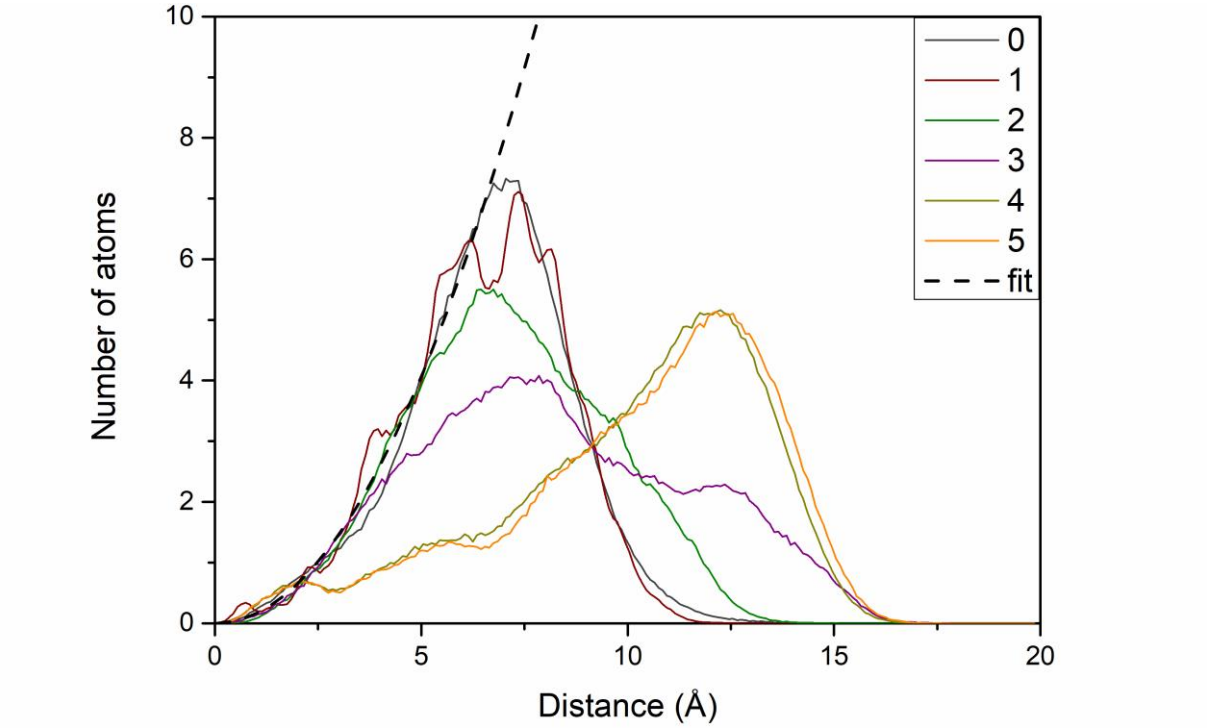

Figure S31: Number of atoms found in concentric shells 0.1 Å thick, as a function of the distance from the geometrical center. Results of PPI G3, for charge states 0 to +5. A parabolic fit corresponding to a dense core model is displayed in dashed lines.

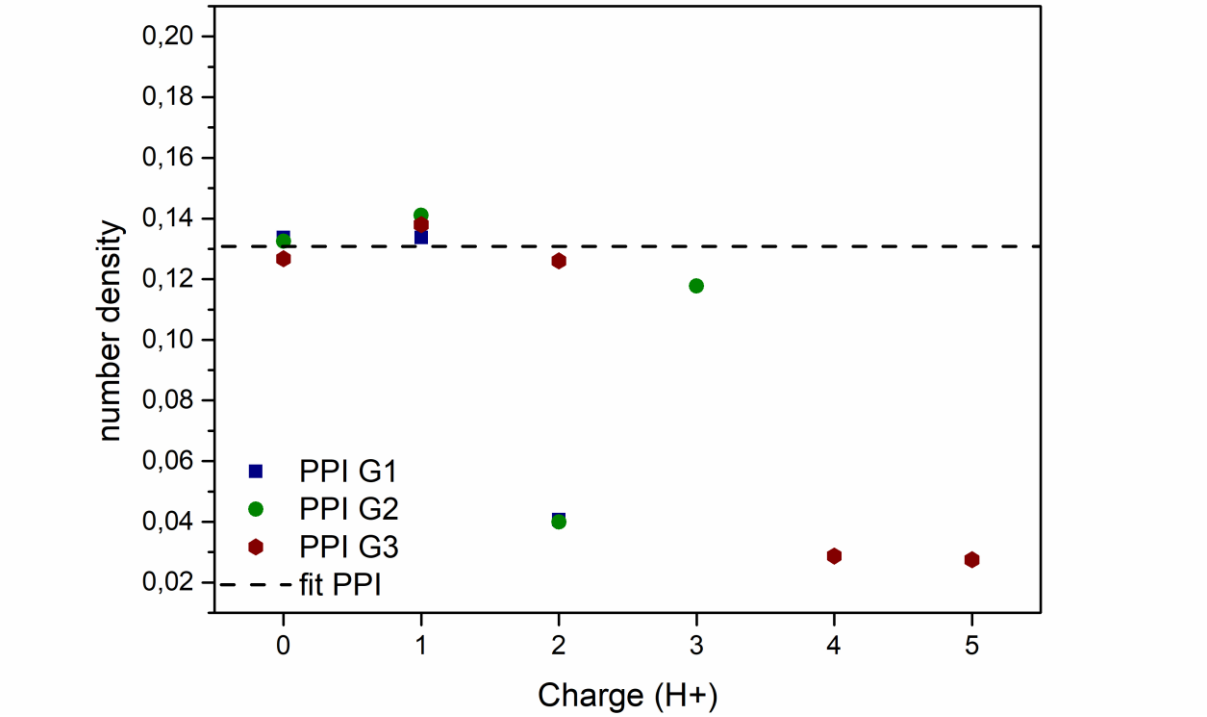

Figure S32: Number density of the dense core for PPI G1 to G3 with different charge states. The average density is represented in dash lines.

Table S6: Comparison between SASA density and apparent density for lowest charge state PPI ions

PPI			
G_x	Charge	ρ_{CCS} (Da/Å^3)	ρ_{SASA} (Da/Å^3)
G1	+1	0.33	0.32
G2	+1	0.30	0.36
G3	+2	0.30	0.40

Equations development

For a sphere with a radius R, a mass M and a density ρ:

$$CCS = \pi R^2 \text{ and } V = \frac{4\pi R^3}{3} = \frac{M}{\rho}$$

$$R = \sqrt[3]{\frac{3M}{4\pi\rho}}$$

$$CCS = \pi\left(\frac{3M}{4\pi\rho}\right)^{2/3}$$

$$CCS = \left(\frac{3\sqrt{\pi}}{4\rho}\right)^{2/3} M^{2/3} = A\, M^{2/3} \text{ (Equation 2)}$$

$$A = \left(\frac{3\sqrt{\pi}}{4\rho}\right)^{2/3}$$

$$A^{3/2} = \frac{3\sqrt{\pi}}{4\rho}$$

$$\rho = \frac{3}{4}\sqrt{\frac{\pi}{A^3}} \qquad \text{(Equation 3)}$$

Parabolic fitting of RDF:

$$N(R \rightarrow R + \Delta R) = n\, V\, (R \rightarrow R + \Delta R) \text{ (Equation 4)}$$

The volume (V) of a spherical shell between R and R + ΔR is the difference between the volume of the sphere of radius R + ΔR and the inner sphere of radius R as given by:

$$V(R \rightarrow R + \Delta R) = \frac{4\pi}{3}(R + \Delta R)^3 - \frac{4\pi}{3}R^3$$

$$V(R \rightarrow R + \Delta R) = \frac{4\pi}{3}(3R^2\Delta R + 3R(\Delta R)^2 + (\Delta R)^3)$$

In our calculations, the shell thickness is set at 0.1Å, so ΔR can be replaced by 0.1 to give:

$$V(R \rightarrow R + \Delta R) = 4\pi\left(0.1\, R^2 + 0.01\, R + \frac{0.001}{3}\right)$$

This equation together with equation 4 give the evolution of the number of atoms as a function of the distance for a homogeneous sphere.

$$N(R \rightarrow R + \Delta R) = n\, 4\pi\left(0.1\, R^2 + 0.01\, R + \frac{0.001}{3}\right) \text{ (Equation 5)}$$

Ion mobility parameters

Table S7: TWIMS parameters for PAMAM G0 and PPI G1

Set	Mass range	IMS Gas Flow (mL.min^{-1})	IMS Wave Velocity (m.s^{-1})	IMS Wave Height (V)
1	100 - 4000	95	950	40
2	100 - 4000	75	800	40
3	100 - 4000	70	850	40
4	100 - 2000	85	900	40
5	100-2000	80	800	40

Table S8: TWIMS parameters for other ions

Set	Mass range	IMS Gas Flow (mL.min^{-1})	IMS Wave Velocity (m.s^{-1})	IMS Wave Height (V)
1	100 - 4000	75	800	40
2	100 - 4000	70	850	40
3	100 - 2000	60	650	40

DRIFT TUBE EXPERIMENTS

$^{DT}CCS_{He}$ are measured using a custom DTIMS instrument described elsewhere [2,3]. The drift tube measures 79 cm and is filled with a constant helium pressure of 5.1 Torr at 295 K. Spectra are recorded with voltage between 200 and 600 V.

REFERENCES

(1) Giordanengo, R.; Mazarin, M.; Wu, J.; Peng, L.; Charles, L. Propagation of Structural Deviations of Poly(Amidoamine) Fan-Shape Dendrimers (Generations 0-3) Characterized by MALDI and Electrospray Mass Spectrometry. *Int. J. Mass Spectrom.* **2007**, *266* (1–3), 62–75.

(2) Simon, A. L.; Chirot, F.; Choi, C. M.; Clavier, C.; Barbaire, M.; Maurelli, J.; Dagany, X.; MacAleese, L.; Dugourd, P. Tandem Ion Mobility Spectrometry Coupled to Laser Excitation. *Rev. Sci. Instrum.* **2015**, *86* (9).

(3) Choi, C. M.; Simon, A.; Chirot, F.; Kulesza, A.; Knight, G.; Daly, S.; MacAleese, L.; Antoine, R.; Dugourd, P. Charge, Color, and Conformation: Spectroscopy on Isomer-Selected Peptide Ions. *J. Phys. Chem. B* **2016**, *120* (4), 709–714.